

Hydrothermal Synthesis of Lignin-Based Carbon Microspheres as Anode Material for Lithium-Ion Batteries

Liping Fan^{1,*}, Linlin Fan², Tao Yu¹, Xin Tan¹, Zhiqiang Shi^{2,*}

¹ School of Chemical Engineering and Technology, Tianjin University, Tianjin 300350, P. R. China

² Tianjin Key Laboratory of Advanced Fibers and Energy Storage. College of Materials Science and Engineering, Tiangong University, Tianjin 300387, P. R. China

*E-mail: 040125@tju.edu.cn (Liping Fan), shizhiqiang@tjpu.edu.cn (Zhiqiang Shi)

Received: 7 September 2019 / Accepted: 7 November 2019 / Published: 31 December 2019

Lignin-based carbon microspheres (LNCS) with regular morphology, good dispersity and uniform particle size were successfully synthesized by hydrothermal method under acidic condition for the first time. LNCS can be prepared by directly carbonization without pre-oxidation. The surface morphology and microcrystalline structure of LNCS was characterized by SEM, TEM and XRD. The structural results show that LNCS possess good sphericity with large interlayer spacing and small graphite-like crystallite size. The electrochemical test results demonstrate that LNCS carbonized at 900°C (LNCS-900) as anode for lithium-ion batteries exhibits the highest specific capacity (180.6 mAh g⁻¹ at 20 mA g⁻¹) and good capacity retention of 98% after 100 cycles. The specific capacity of LNCS-900 recovers from 48.9 mAh g⁻¹ to 171.8 mAh g⁻¹ as the current density decreases from 1 A g⁻¹ to 20 mA g⁻¹, displaying excellent rate performance. Therefore, the as-prepared LNCS is a potential promising and low-cost anode material for lithium-ion batteries.

Keywords: Lignin; Hydrothermal method; Carbon microspheres; Hard carbon; Lithium-ion battery

1. INTRODUCTION

In the past few decades, social development has been heavily dependent on fossil energy, leading to serious environmental pollution, such as the greenhouse effect, haze and acid rain. Scientists continue to develop green energy (solar, wind, tidal, etc.) to replace fossil energy while meeting the energy needs of social development. But the development of these new energy is limited by their regional and intermittent nature. Therefore, reliable and effective energy storage technologies have become the key solution. Electrochemical storage energy technology based on secondary battery has significant advantages because of their high capacity, long cycle life, lowcost and high safety [1-2]. Lithium-ion batteries (LIBs) have been rapidly developed in electronic products and electric vehicles due to the

strength of high voltage, high energy density and long cycle life, which greatly promoted the application of new energy storage electrode materials and new technology system [3-4]. The need for LIBs in transport industries increasingly call for high power density and excellent rate capability. Carbonaceous materials are widely used as anode materials for LIBs due to its structural and chemical stability, long cycle life, low cost and abundant precursors [5-6]. Commercial graphite has a small specific capacity (372mAh g^{-1}) and poor rate performance. Compared with graphite, hard carbon has advantages of high specific capacity, long durability and outstanding low temperature performance [7-8].

Now, many reports on hard carbon anode have reported many methods for preparing hard carbon. Bitumen [9], anthracite [10], glucose [11], sucrose [12-13], phenolic resins [14] and various biomass [15-18] are often used as hard carbon precursor, but such hard carbon anode either exhibits small initial coulombic efficiency (ICE) or increases production cost. Lignin, the second most abundant polymer in nature, is considered to be a suitable precursor for the preparation of hard carbon due to the advantages of low cost, avirulence, renewability and high aromatic carbon content [19-20]. However, the hard carbon with turbostratic structure often endure low conductivity compared with graphite and soft carbon thus limits its electrochemical performance in LIBs [21]. Some researchers have applied electrospinning method to prepare carbon nanofibers using lignin as carbon source [22-24]. *Choi* [25] prepared PAN/lignin nanofiber electrode by electrospinning and improved the performance as anode for LIBs. Although this method can establish a 3D conductive network with good electrochemical performance, the synthesis process is too complicated to achieve large-scale industrial production. Carbon microspheres (CMS) are very suitable as anode material for secondary batteries due to its adjustable microstructure, easy dispersion in slurry, causing densely packing along with enough interspace for effective electrolyte transportation [26-27]. So far, it has been challenging to prepare uniformly dispersed CMS with uniform size.

In this paper, we attempt to use an easy, economical and fast route to prepare lignin-based carbon microspheres (LNCS) by hydrothermal synthesis and carbonization reaction. The characteristics of good monodisperse, sphericity and high packing density effectively improve the energy storage performance of LNCS as anode for LIBs, especially on long cycle stability.

2. EXPERIMENTAL

2.1 Materials synthesis

Sodium lignosulphonate was added to hydrochloric acid solution under stirring. After completely dissolving, the solution was transferred to Teflon-lined stainless steel autoclave and treated at 250°C for 60 h. After centrifugation, LNCS was dried at 60°C for 12 h. Then hydrothermal microspheres were carbonized at 900°C , 1100°C , 1300°C , 1500°C under Ar/H_2 (95:5, v/v) atmosphere for 3h. The resulting samples were denoted as LNCS-x (x= 900, 1100, 1300, 1500).

2.2. Material characterizations

The morphology and pore structure was observed by scanning electron microscopy (SEM, Hitachi S4800) and Brunauer Emmette Teller (BET). X-ray diffraction patterns (XRD) of samples were measured with a Rigaku D/Max2500 X-ray diffractometer using Cu K α radiation. Raman spectra was recorded on an XploRA plus Horiba spectrometer, with an excitation laser wavelength of 523 nm. The surface state and chemical composition of the samples were analyzed by X-ray photoelectron spectroscopy (XPS).

2.3. Electrochemical measurement

The slurry was prepared by mixing LNCS-x, acetylene black, and PVDF with a mass ratio of 87:5:8. Then the slurry was pasted onto copper foil. The parameters of the disc electrode are as followings: diameter, Φ 13 mm; surface area, 1.327 cm²; mass, 4.0 mg; thickness, 50 μ m. Coin-type cells (CR2430) were assembled in argon-filled glove box with the working electrode, electrolyte (1 M LiPF₆ dissolved in EC/DEC (1:1, v/v)), separator (polyethylene). Cyclic voltammetry (CV) testing was performed on a CHI604a electrochemical workstation (Chenhua Instrument Company, Shanghai, China) at a scan rate of 0.1 mVs⁻¹. The specific capacity, rate capacities, coulomb efficiency and cycle stability of the Li-ion batteries were conducted on a multi-channel Land Battery Test System at the range of 0.01-3 V.

3. RESULTS AND DISCUSSION

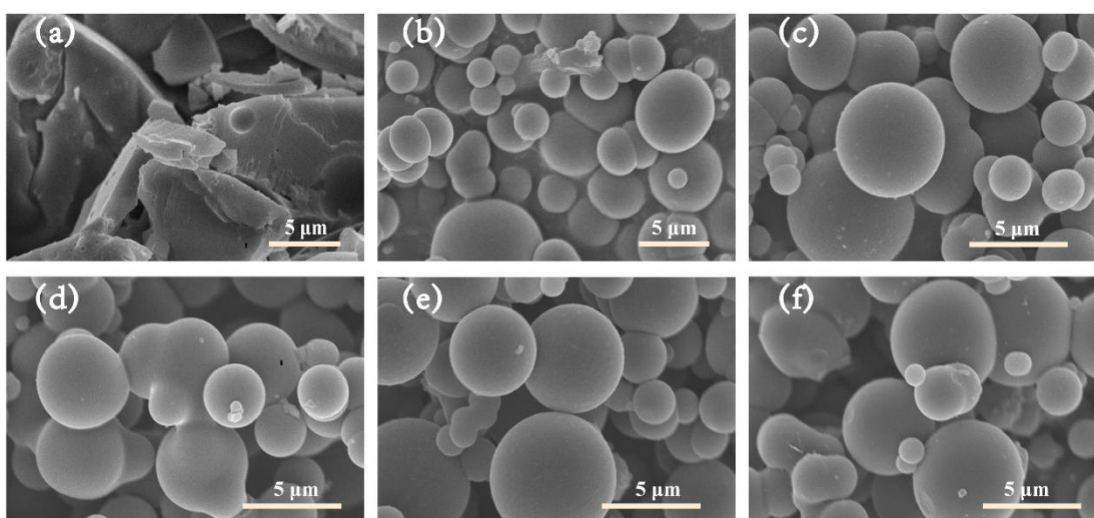


Figure 1. SEM images of (a) raw material; (b)hydrothermal carbon microspheres; (c)LNCS-900; (d)LNCS-1100; (e)LNCS-1300; and (f)LNCS-1500.

As depicted in Figure 1a, raw material shows a irregular morphology with the average diameter of 1~20 μ m. In this study, LNCS were prepared through hydrothermal reaction under acid condition, as

shown in Fig 1b. The process of LNCS formation consists of a series of chemical reactions such as thermal decomposition and thermal condensation reaction [28-29]. The acid condition plays an important role in the formation process of LNCS.

The as-obtained LNCS have smooth surface and disperse well with a small amount of agglomeration and have uniform partial size of 3-5 μm . In comparison, other carbon microspheres have wide size distribution, severe aggregation or fusion happens in many studies [30]. The small particle size helps to reduce the diffusion distance of lithium ions, and the monodisperse spherical morphology can offer more paths for the transport of electrolyte. After carbonization, the microspheres still keep sphericity and smooth surface well without breakage and melting, as shown in Fig. 1c-f.

Fig. 2 shows the XRD patterns and Raman spectra of LNCS-x. The values of structure parameters are summarized in Table 1. Two broad peaks locate near 23.5° and 43°, corresponding to (002) and (100) diffraction peak of typical amorphous carbon [31], as shown in Fig. 2a. With carbonization temperature increasing microcrystallite size (L_c and L_a) increases, while the interlayer distance (d_{002}) value decreases from 0.381 to 0.370, indicating that high temperature carbonization can improve the growth of internal carbon hexagonal network plane and graphite-like microcrystallite units thus increasing graphitization degree. Raman spectra shows the similar results in Fig. 2b. Raman spectra of LNCS-x have two broad peaks located at 1340 cm^{-1} (D-band) and 1580 cm^{-1} (G-band). D-band represents the defects and G-band is related to the E_{2g} vibration of graphite crystallite. The decrease of half width and better symmetry of the two band indicate an increase in the degree of graphitization. As listed in Table 1, the integrate intensity ratio of D-band and G-band, (I_D/I_G), decreases with carbonization temperature increase, indicating that the defect structure of inner crystallite-like decreases, while the crystalline structure increase [32].

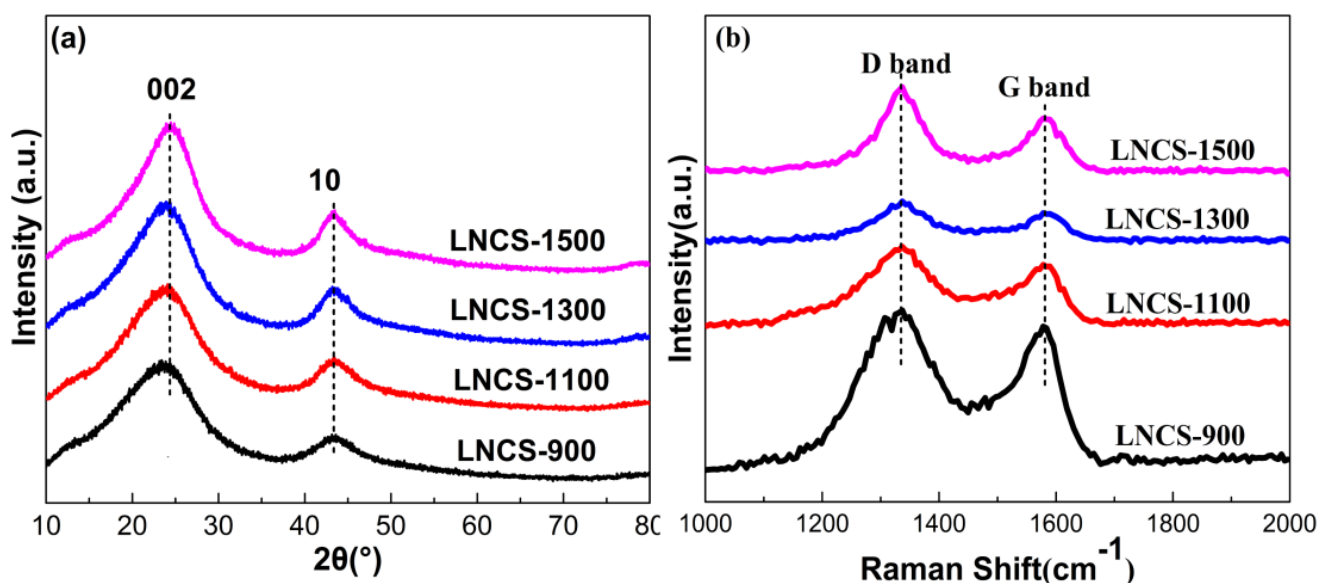


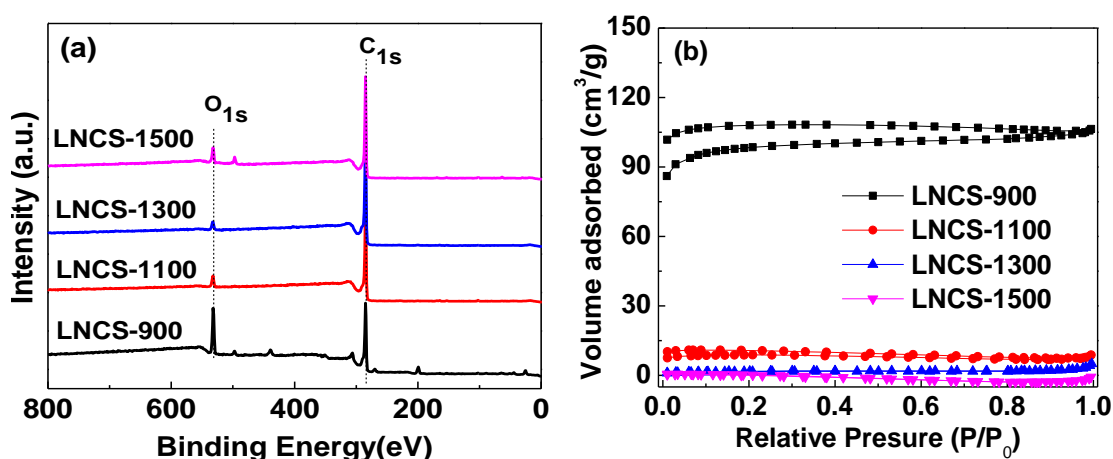
Figure 2. XRD patterns and Raman spectra of LNCS-x.

Table 1. Structural parameters of LNCS-x

Samples	d_{002} /nm	L_c /nm	L_a /nm	N	R (I_D/I_G)	S_{BET}^* (m^2/g)	Pore volume (cm^3/g)
LNCS-900	0.381	1.679	3.951	5	2.660	327.990	0.165
LNCS-1100	0.378	1.743	4.090	6	2.525	29.345	0.014
LNCS-1300	0.378	1.750	4.142	6	1.584	5.878	0.008
LNCS-1500	0.370	2.050	4.561	6	1.459	0.497	0.003

* S_{BET} is calculated by BET method.

X-ray photoelectron spectroscopy (XPS) survey scan spectra of LNCS-x are shown in Fig. 3a. A conspicuous XPS C1s peak at $\sim 286eV$ and an O1s peak at $\sim 534eV$ are present in the four samples, as shown in Fig. 3a. It confirms that all samples are mainly composed of C and O elements. With the carbonization temperature increasing, the oxygen content decreases significantly while the carbon content increases. The specific surface area (SSA), pore size distribution and porosity structure are further analyzed by N_2 adsorption-desorption measurement. As shown in Fig. 3b, the adsorption-desorption curves of LNCS-x are typical type-I isotherms, indicating that the samples is predominantly microporous. The formation of micropore may be due to the decrease of functional groups, volatilization of small molecules and uneven shrinkage of matrix [33]. The SSA is directly connected with the carbonization temperature. The SSA decreases with the increase of carbonization temperature. As shown in Table 1, LNCS-900 possesses the largest SSA of $327.990 m^2 g^{-1}$, while LNCS-1100, LNCS-1300, LNCS-1500 shows small SSA of 29.345, 5.878 and $0.497 m^2 g^{-1}$.

**Figure 3.** (a) XPS and (b) N_2 adsorption-desorption curves of LNCS-x.

The cyclic voltammetry (CV) curves of LNCS-x at a scanning rate of $0.1mV s^{-1}$ between the voltage range of 0-3V are shown in Fig. 4. Two apparent peaks appear at 1.25-0.5 V and 0.2-0 V in the first cathodic cycle. The cathodic peak at 1.25-0.5V only appears in the first cycle, which is ascribed to

the formation of solid electrolyte interphase (SEI) films and the irreversible reaction of electrolyte on electrodes surface [34]. A pair of redox peaks at 0.2-0 V corresponds to insertion/extraction of Li-ion at the graphite domain. Subsequent CV curves overlap very well, indicating that the insertion and extraction of Li-ion is reversible well in the LNCS-x electrodes.

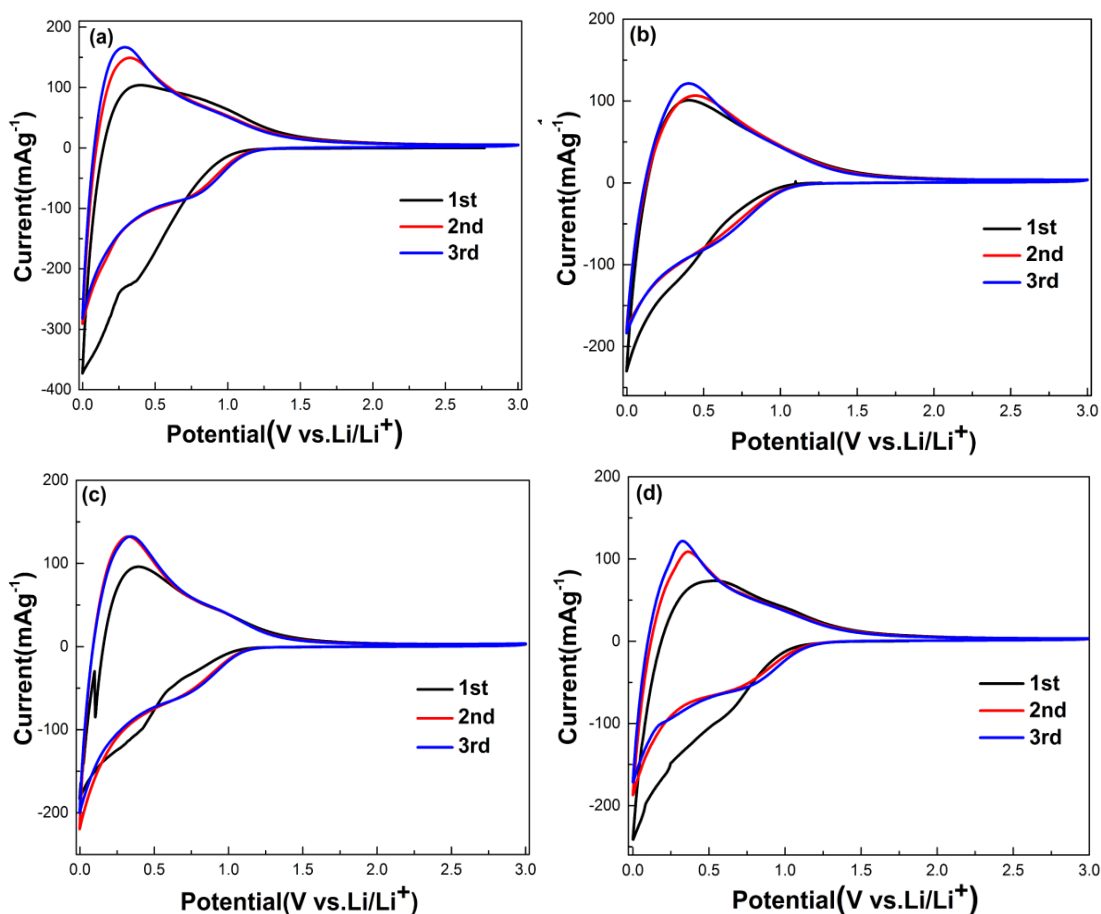


Figure 4. CV curves of (a) LNCS-900; (b) LNCS-1100; (c) LNCS-1300; and (d) LNCS-1500.

The galvanostatic charge/discharge profiles of the first cycle of the LNCS-x electrodes at a current density of 20 mA g^{-1} is showed in Fig. 5. The relation of voltage and specific capacity for LNCS-x is linear, and the charge-discharge curves display typical "V" type. The initial discharge specific capacity of LNCS-900 is 341.9 mAh g^{-1} , and the initial coulombic efficiency (ICE) is 52.8%. The ICE increase with the carbonization temperature increasing, which is ascribed to the decrease of defects, SSA and oxygen-containing functional groups. The irreversible capacity loss of LNCS-x in the first discharge process is imputed to the formation of SEI layers and some side reaction on the surface of electrode [35-36].

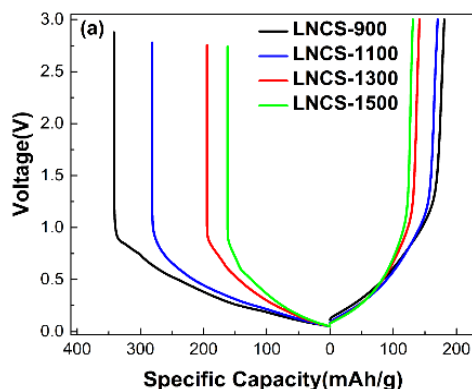


Figure 5. Galvanostatic charge/discharge curves of LNCS-x at current density of 20 mA g⁻¹ for the first cycle.

The rate capability and cycle performance of LNCS-x as anode material in LIBs are shown in Fig. 6. LNCS-900 exhibits a better rate performance than other samples under different current densities. LNCS-900 delivers reversible charge capacity of 180.3, 148.4, 127.7, 121.1, 87.4, 61.4, 53.2 mAh g⁻¹ at 20, 50, 100, 200, 500, 750, 1000 mA g⁻¹, respectively. As a comparison, LNCS-1500 exhibits a much inferior rate performance. The samples suffered high temperature carbonization have a smaller interlayer distance than the samples at low temperature carbonization meanwhile the defects are decreased, which is not conducive to the rapid insertion of Li-ions, thus causing the inferior rate performance. The long-term cycling performance of LNCS-x at 100mA g⁻¹ was tested. As shown in Fig. 6b, the LNCS-900 exhibits the highest reversible capacity of 169mAh g⁻¹ with the retention of 98% after 100 cycles, indicating excellent Li-ion insertion-extraction stability. As a comparison, LNCS-1100, LNCS-1300, LNCS-1500 only delivered a capacity of 134, 122, 107 mAh g⁻¹, much low lame to LNCS-900, indicating the defects and active sites are more suitable to storage Li-ions.

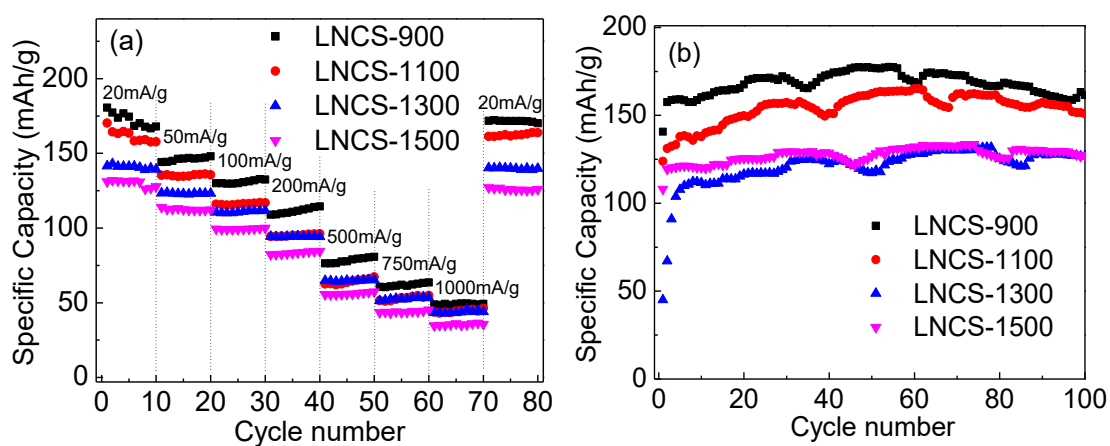


Figure 6. (a) Rate capability of LNCS-x from 20 mA g⁻¹ to 1A g⁻¹; (b) Cyclic performance of LNCS-x at a current rate of 100 mA g⁻¹.

4. CONCLUSION

In summary, uniform lignin-based carbon microspheres were successfully prepared through hydrothermal method. The obtained samples have excellent dispersibility, regular sphericity and uniform particle size. The carbonized temperature doesn't affect the morphology of LNCS, but directly affects the microscopic structure such as the size of graphite-like crystallite, interlayer distance, specific surface area and pore volume. The LNCS carbonized at 900 °C shows the highest charge/discharge capacity, the best rate capability, and long-term cycle life as anode material in LIBs. The simple hydrothermal method using the cheap and green precursor is a promising method for the preparation of carbon material.

ACKNOWLEDGMENTS

This research was financially supported by Tianjin application foundation, advanced technology research plan project (15ZCZDGX00270, 14RCHZGX00859) and Tianjin university independent innovation foundation (1705).

References

1. B. Dunn, H.Kamath, J. M.Tarascon, *Science*, 334(2011)928.
2. D. Larcher, J.M. Tarascon, *Nat. Chem.*, 7(2015)19.
3. C.-X. Zu, H. Li, *Energy Environ. Sci.*, 4(2011)2614.
4. J. Zheng, Y. Hou, Y. Duan, X. Song, Y. Wei, T. Liu, J. Hu, H. Guo, Z. Zhuo and L. Liu, *Nano lett.*, 15(2015)6102.
5. T. Iijima, K. Suzuki, Y. Matsuda, *Synth. Met.*, 73(1995)9.
6. Y.P. Wu, E. Rahm, R. Holze, *J.Power Sources*, 114(2003)228.
7. K. Gotoh, M. Maeda, A. Nagai, A. Goto, M. Tansho, K. Hashi, T. Shimizu, H. Ishida, *J.Power Sources*, 162(2006)1322.
8. D. Stevens and J. Dahn, *J. Electrochem. Soc.*, 147(2000)1271.
9. Y. Li, Y. S. Hu, H. Li, L. Chen and X. Huang, *J. Mater. Chem.A.*, 4(2016)96.
10. Y. J. Kim, H. Yang, S. H. Yoon, Y. Korai, I. Mochida and C. H. Ku, *J. Power Sources*, 113 (2003)157.
11. R. Väli, A. Jänes, T. Thomberg and E. Lust, *Electrochimi. Acta*, 253(2017)536.
12. J. Yang, X.Y. Zhou, J. Li, Y.L. Zou, J.J. Tang, *Mater. Chem. Phys.*, 135(2012)445.
13. G.T.K. Fey, Y.C. Kao, *Mater. Chem. Phys.*, 73(2002)37.
14. H. L. Wang, Z. Q. Shi, J. Jin, C. B. Chong and C. Y. Wang, *J. Electroanal. Chem.*, 755 (2015)87.
15. G.T.K. Fey, C.L. Chen, *J. Power Sources*, 97–98(2001).
16. G.T.K. Fey, D.C. Lee, Y.Y. Lin, T.P. Kumar, *Synth. Met.*, 139(2003)71.
17. Y.J. Hwang, S.K. Jeong, J.S. Shin, K.S. Nahm, A.M. Stephan, *J. Alloy. Compd.*, 448 (2008)141.
18. S.W. Han, D.W. Jung, J.H. Jeong, E.S. Oh, *Chem. Eng. J.*, 254(2014)597.
19. W.J.J. Huijgen, G. Telysheva, A. Arshanitsa, R.J.A. Gosselink, P.J. de Wild, *Ind. Crop. Prod.*, 59(2014)85.
20. A.U. Buranov, G. Mazza, *Ind. Crop. Prod.*, 28(2008)237.
21. B. Zhang, F. Kang, J.M. Tarascon, J. Kim, *Prog. Mater. Sci.*, 76(2016)319.
22. D.I. Choi, J.N. Lee, J. Song, P.H. Kang, J.K. Park, Y.M. Lee, *J. Solid State Electrochem.* 17(2013)2471.
23. J. Jin, B.J. Yu, Z.Q. Shi, C.Y. Wang, C.B. Chong, *J. Power Sources*, 272(2014)800.
24. S.X. Wang, L. Yang, L.P. Stubbs, X. Li, C. He, *ACS Appl. Mater. Interfaces*, 5(2013) 12275.
25. D. I. Choi, J. N. Lee, J. Song, P. H. Kang, J. K. Park and Y. M. Lee, *J. Solid State Electrochem.*,

- 17(2013)2471.
26. R. Fu, Z. Chang, C. Shen, H. Guo, H. Huang, Y. Xia, Z. Liu, *Electrochim. Acta*, 260 (2018)430.
27. H. W. Zhang, M.X. Hu, Q. Lv, L. Yang, R. T. Lv. *Electrochimica Acta*, 297(2019) 365.
28. H. Wikberg, T. Ohraaho, F. Pileidis and M.-M. Titirici, *ACS Sustain Chem Eng*, 2015, 3:150927224922009.
29. D.S. Bin, Z.X. Chi, Y. Li, K. Zhang, X. Yang, Y.G. Sun, J.Y. Piao, A.M. Cao, L.J. Wan, *J. Am. Chem. Soc.*, 139 (2017) 13492.
30. G. Wen, B. Wang, C. Wang, J. Wang, Z. Tian, R. Schlögl, D.S. Su, *Angew. Chem.* 129 (2016) 615.
31. Y.R. Qi, Y.X. Lu, F.X. Ding, Q.Q. Zhang, H. Li, X.J. Huang, L.Q. Chen, Y.S. Hu, *Angew. Chem.* 58 (2019) 4361.
32. A.C. Ferrari, J. Robertson, *J. Philos. Trans. R. Soc. A*, 362 (2004) 2477.
33. Y.Y. Zhu, M.M. Chen, Q. Li, C. Yuan, C.Y. Wang, *Carbon*, 129 (2018) 695.
34. W.L. Zhang, J. Yin, Z.Q. Lin, H.B. Lin, H.Y. Lu and Y. Wang, *Electrochimi. Acta*, 176 (2015) 1136.
35. Y. Matsumura, S. Wang, J. Mondori, *J. Electrochem. Soc.*, 142 (9) (1995).
36. Z.Z. Chang, B.J. Yu, C.Y. Wang, *Electrochimi. Acta*, 176 (2015) 1352.

© 2020 The Authors. Published by ESG (www.electrochemsci.org). This article is an open access article distributed under the terms and conditions of the Creative Commons Attribution license (<http://creativecommons.org/licenses/by/4.0/>).